

Combinatorial Responses Controlled by Synaptic Inhibition in the Cerebellum Granular Layer

Jonathan Mapelli, Daniela Gandolfi and Egidio D'Angelo

J Neurophysiol 103:250-261, 2010. First published 11 November 2009; doi:10.1152/jn.00642.2009

You might find this additional info useful...

Supplemental material for this article can be found at:

<http://jn.physiology.org/content/suppl/2009/11/09/00642.2009.DC1.html>

This article cites 63 articles, 31 of which can be accessed free at:

<http://jn.physiology.org/content/103/1/250.full.html#ref-list-1>

Updated information and services including high resolution figures, can be found at:

<http://jn.physiology.org/content/103/1/250.full.html>

Additional material and information about *Journal of Neurophysiology* can be found at:

<http://www.the-aps.org/publications/jn>

This information is current as of January 31, 2011.

Combinatorial Responses Controlled by Synaptic Inhibition in the Cerebellum Granular Layer

Jonathan Mapelli,* Daniela Gandolfi,* and Egidio D'Angelo

Department of Physiology, University of Pavia and National Consortium for the Physics of Matter, Pavia, and Brain Connectivity Center, Istituto Neurologico IRCCR Fondazione C. Mondino, Pavia, Italy

Submitted 22 July 2009; accepted in final form 5 November 2009

Mapelli J, Gandolfi D, D'Angelo E. Combinatorial responses controlled by synaptic inhibition in the cerebellum granular layer. *J Neurophysiol* 103: 250–261, 2010. First published November 11, 2009; doi:10.1152/jn.00642.2009. The granular layer of cerebellum has been long hypothesized to perform combinatorial operations on incoming signals. Although this assumption is at the basis of main computational theories of cerebellum, it has never been assessed experimentally. Here, by applying high-resolution voltage-sensitive dye imaging techniques, we show that simultaneous activation of two partially overlapping mossy fiber bundles (either with single pulses or high-frequency bursts) can cause combined excitation and combined inhibition, which are compatible with the concepts of coincidence detection and spatial pattern separation predicted by theory. Combined excitation appeared as an area in which the combination of two inputs is greater than the arithmetic sum of the individual inputs and was enhanced by γ -aminobutyric acid type A (GABA_A) receptor blockers. Combined inhibition was manifest as an area where two inputs combined resulted in a reduction to less than half of the activity evoked from either one of the two inputs alone and was prevented by GABA_A receptor blockers. The combinatorial responses occupied small granular layer regions (~ 30 μ m diameter), with combined inhibition being interspersed among extended areas of combined excitation. Moreover, the combinatorial effects lasted for tens of milliseconds and combined inhibition occurred only after termination of the stimuli. These combinatorial operations, if engaged by natural input patterns *in vivo*, may be important to influence incoming impulses organizing spatiotemporal spike sequences to be relayed to Purkinje cells.

INTRODUCTION

In addition to single-neuron properties, specific network connectivity is expected to play a critical role for circuit computation (Buzsáki 2006; Churchland and Sejnowski 1992; McNaughton et al. 1989). In the hippocampal dentate gyrus, which preprocesses perforant-path signals to be relayed to CA3 neurons, operations like pattern completion and separation have been reported (Bakker et al. 2008; Fyhn et al. 2007; Galvan et al. 2008; Leutgeb et al. 2007). In the cerebellum granular layer, incoming neural signals are preprocessed before being relayed to the Purkinje cells (Eccles et al. 1967). It was suggested that a combinatorial rearrangement of connections would reroute multiple inputs through partially overlapping channels, thus inspiring the idea that the convergence of inputs and lateral inhibition would allow combinatorial operations like coincidence detection and spatial pattern separation (Albus 1971; Fujita 1982; Marr 1969, 1971). Despite their critical importance and recurrent use in cerebellar computational theories (e.g., see Gibson et al. 1991; Torioka 1980; Tyrrell and Willshaw 1992), these properties have not yet undergone experimental assessment.

In the cerebellum granular layer, mossy fibers activate granule cells and Golgi cells generating a feedforward (mossy fiber \rightarrow Golgi cell \rightarrow granule cell) and a feedback (mossy fiber \rightarrow granule cell \rightarrow Golgi cell \rightarrow granule cell) inhibitory loop (Eccles et al. 1967). Mossy fiber convergence onto granule cells and the lateral organization of Golgi cell inhibition (D'Angelo 2008; D'Angelo et al. 1995; Jörntell and Ekerot 2006; Mapelli and D'Angelo 2007) provide a substrate for combinatorial operations (Buzsáki 2006). An important issue concerns circuit dynamics, since phasic inhibition occurs with a delay both in the feedforward and the feedback loops (Kanichay and Silver 2008; Mapelli and D'Angelo 2007) and Golgi cells are endowed with complex time-dependent properties including spike frequency adaptation, rebounds, and silent pauses (Solinas et al. 2007a,b). Thus one should expect that combinatorial operations have specific spatiotemporal dynamics related to the inhibitory loops.

In this work, voltage-sensitive dye (VSD) imaging in acute cerebellar slices allowed us to investigate the effect of mossy fiber double-bundle stimulation at high spatiotemporal resolution. Specific areas of the cerebellum granular layer, with dimensions compatible with anatomically identified functional units (Sultan 2001; Wu et al. 1999), performed either combined excitation or combined inhibition under control of synaptic inhibition. These combinatorial effects appear as the biological counterpart of the theoretical concepts of coincidence detection and spatial pattern separation predicted by theory and may be important to process the mossy fiber input and generate appropriate spike patterns to be relayed to Purkinje cells (Brunel et al. 2004; D'Angelo and DeZeeuw 2009; de Solages et al. 2008; Steuber et al. 2007).

METHODS

Neuronal circuit analysis has recently been fostered by techniques revealing the spatiotemporal organization of activity inside and across neuronal ensembles (Brecht et al. 2004; Buzsáki 2004; Nicoletis et al. 2003). VSD imaging allows one to record electrical activity over extended neuronal circuits with high stability and spatiotemporal resolution (Berger et al. 2007; Cohen and Yarom 1998; Contreras and Llinás 2001; Derdikman et al. 2003; Ferezou et al. 2006; Grinvald and Hildesheim 2004; Tominaga et al. 2000; Zhou et al. 2007). In this work, VSD imaging has been performed in acute cerebellar slices. It should be noted that, although VSD and intrinsic fluorescence techniques have been applied to investigate molecular layer and Purkinje cell responses (Chen et al. 2005; Cohen and Yarom 1998; Ebner et al. 2005; Elias et al. 1993; Rokni et al. 2007; Staub et al. 1994; Yae et al. 1992), the spatiotemporal dynamics of granular layer activation were never previously considered in detail.

Experimental techniques

Acute cerebellar slices were obtained from 18- to 25-day-old Wistar rats as previously reported (D'Angelo et al. 1995, 1999).

* These authors contributed equally to this work.

Address for reprint requests and other correspondence: E. D'Angelo, Department of Physiology, University of Pavia and CNISM, Via Forlanini 6, I-27100 Pavia, Italy (E-mail: dangelo@unipv.it).

Briefly, rats were anesthetized with halothane (Sigma; 0.5 ml in 2 dm³ for 1–2 min) before being killed by decapitation. The cerebellum was gently removed, the vermis was isolated, fixed on a plastic support with cyano-acrylic glue, and immersed into a cold (2–3°C) cutting solution. Slices (220 μm thick) were cut in the sagittal plane. The cutting solution contained (in mM) (Dugué et al. 2005): K-gluconate 130, KCl 15, EGTA 0.2, Hepes 20, and glucose 10 (pH 7.4 with NaOH). Slices were incubated for about 1 h before recordings at 31°C in oxygenated Krebs solution containing (in mM): NaCl 120, KCl 2, MgSO₄ 1.2, NaHCO₃ 26, KH₂PO₄ 1.2, CaCl₂ 2, glucose 11 (pH 7.4 when equilibrated with 95% O₂-5% CO₂). When needed, the extracellular solution was added with the γ -aminobutyric acid type A (GABA_A) receptor blocker, 10 μM bicuculline (Sigma), the *N*-methyl-D-aspartate (NMDA) and α -amino-3-hydroxy-5-methyl-4-isoxazolepropionic acid (AMPA) receptor blockers, 50 μM D-2-amino-5-phosphonovaleric acid (D-APV or simply APV; Tocris Cookson), and 10 μM 2,3-dihydroxy-6-nitro-7-sulfamoyl-benzo-[f]quinoxaline-2,3-dione (NBQX; Tocris Cookson). The dye (Di-4-ANEPPS; Molecular Probes) was dissolved and stocked in Krebs with 50% ethanol (Sigma) and 5% Cremophor EL (a castor oil derivative; Sigma). Slices for optical recordings were incubated for 30 min in oxygenated Krebs solution added with 3% Di-4-ANEPPS stock solution mixed with 50% fetal bovine serum (Molecular Probes).

Slices were gently positioned in the recording chamber and were immobilized with a nylon mesh attached to a platinum Omega wire to improve tissue adhesion and mechanical stability. Perfusion of standard extracellular solution (2–3 ml/min) maintained at 32°C with a feedback temperature controller (Thermostat HC2, Multi Channel Systems, Reutlingen, Germany) was performed during the recording session. In most experiments, the chamber embedded a multielectrode array for simultaneous recording and stimulation (MEA 60 Multi Channel Systems; see Mapelli and D'Angelo 2007 for further details). In some experiments, VSD was combined with whole cell recordings (WCRs; for details see Nieuws et al. 2006). The MEA and VSD signals showed a clear congruence (cf. Fig. 1), demonstrating the effectiveness of VSD in detecting membrane potential changes. Moreover, granule cell excitation in WCRs correlated with the VSD signal (cf. Fig. 2). MEA and WCRs performed on granule cells did not reveal any significant difference between stained and unstained slices in terms of electrophysiological parameters (data not shown; see also Staub et al. 1994; Tominaga et al. 2000).

The mossy fibers were stimulated with square voltage pulses (± 4 –8 V; 200 μs) delivered either individually or in trains (100 or 500 Hz). Voltage pulses were usually applied through couples of MEA electrodes (STG 1008, Multi Channel Systems). The advantage of this arrangement was that the 60 MEA electrodes allowed us to select multiple stimulation sites in the same experiment. During coupled VSD and patch-clamp recordings, stimulation was performed by using a bipolar tungsten electrode connected to a pulse generator through a stimulus isolation unit.

VSD recordings and VSD signals

The recording chamber was installed on an upright epifluorescence microscope (BX51WI, Olympus, Europa, Hamburg, Germany), equipped with a $\times 10$ (UM Plan FL 0.3 numerical aperture [NA]) or $\times 60$ (LUM Plan FL 0.9 NA) objective (see Tominaga et al. 2000). The light generated by a halogen lamp (150 W, MHF-G150LR, Moritex, Tokyo, Japan) controlled by an electronic shutter (model 0, Copal, Tokyo, Japan) was passed through an excitation filter ($\lambda = 530 \pm 10$ nm), projected onto a dichroic mirror ($\lambda = 565$ nm), and reflected toward the objective lens to illuminate the specimen. Fluorescence generated by the tissue was transmitted through an absorption filter ($\lambda > 590$ nm) to the charge-coupled detector (CCD) camera (MICAM01, Scimedia, Brainvision, Tokyo, Japan). The whole imaging system was connected through an I/O interface (MICAM01, Brainvision) to a PC controlling illumination, stimulation, and data

acquisition. Given the MICAM01 chip resolution (64 \times 96 pixels, each with 30 \times 30-μm² surface), the $\times 10$ objective and the $\times 0.35$ C-mount adapter, the final magnification was $\times 3.5$, yielding an imaging area of 579 \times 850 μm² and a pixel size of about 9 \times 9 μm². Full-frame image acquisition was performed at 1 kHz. Data were acquired and displayed by Brainvision software and signals were analyzed using routines written in MATLAB (The MathWorks, Natick, MA) and IGOR Pro (WaveMetrics, Lake Oswego, OR).

At the beginning of recordings, a calibration procedure was adopted to ensure homogeneity across experiments. The dynamic range of the CCD camera was calibrated by measuring background fluorescence and setting the average light intensity in the absence of stimulation to 60% of the saturation level. When VSD acquisition was started, the optical baseline was sampled for 55 ms before triggering electrical stimulation. The baseline was used to measure the initial fluorescence intensity (F_0) by averaging eight consecutive frames. The relative fluorescence change (ΔF) was then calculated for each timeframe and data analysis was performed on $\Delta F/F_0$ values. The stimulation intensity was chosen so that the maximum granular layer response measured 0.5–1% $\Delta F/F_0$. VSD signal analysis was performed on the initial 70 min of the experiments, during which F_0 remained almost stable, indicating little photobleaching (Fig. 1B).

The signal-to-noise (S/N) ratio was improved by averaging 16 consecutive acquisitions at the stimulus repetition frequency of 0.2 Hz. Given maximal $\Delta F/F_0 \cong 1\%$ and noise SE $\cong \pm 0.1\%$ ($n = 12$ slices), the S/N ratio was about 10-fold, ensuring a reliable measurement of peak response amplitude. The VSD fluorescence depends on the relative surface and density of the electrogenic elements of the granular layer. The granule cell/Golgi cell ratio is 500:1 for number of cells (Eccles et al. 1967; Harvey and Napper 1991) and 3:50 for cell surface (D'Angelo et al. 1999; Dieudonné 1998). This yields a 30-fold larger electrogenic surface for granule cells, which thus had to determine most of the signal.

Following stimulation, $\Delta F/F_0$ reached its maximum amplitude in 3–5 ms, corresponding to the early component of the local field potential (N_{2a} wave) and to the first granule cell spike (Fig. 2; cf. Mapelli and D'Angelo 2007). The VSD was therefore able to reveal the occurrence of spikes in the appropriate time window. After about 5 ms, circuit inhibition depresses granule cell responses. Thus analysis of the effects of excitation and inhibition could be performed in 5-ms periods (i.e., by averaging five consecutive acquisition frames) beginning with the stimulus. This temporal averaging procedure provided a further S/N improvement without introducing significant error in terms of granule cell firing control (see Figs. 5–8 and Supplemental Material).¹

The correlation between VSD signals and neuron membrane potential changes was analyzed by performing simultaneous WCRs from granule cells (as in Mapelli and D'Angelo 2007). To this aim, the VSD signals were collected from 16 binned pixels arranged in a 4 \times 4 array and a granule cell was recorded from the core of the same area (Fig. 2, A and B). This comparison showed a direct nearly linear relationship between intracellular membrane potential and VSD signal. It should be noted that, since the VSD signal was 1) collected from numerous granule cells, 2) averaged over several acquisitions, and 3) sampled at 1 frame/ms, it could not reveal the precise shape of the action potential (e.g., the fast rise and subsequent afterhyperpolarization [AHP]). The VSD signal was modulated by the contribution of the excitatory glutamate NMDA and AMPA receptors and by the inhibitory GABA_A receptor (see Fig. 3 for details), revealing its sensitivity to subthreshold integration of synaptic inputs.

Data analysis: threshold setting and noise evaluation

An automatic spot selection procedure was implemented to remove subjectivity and to efficiently extend analysis over all spots and all experiments. The granular layer response to single (R_{S1} , R_{S2}) and double stimuli ($R_{S1\&S2}$) was compared with a threshold set at 35% of

¹ The online version of this article contains supplemental data.

the maximum normalized response (T_{35}) to discriminate signals from noise. A second threshold was set at 70% of the maximum normalized response (T_{70}) to identify strongly responding regions (see Fig. 2). Combined excitation was identified as the case in which

$$\begin{cases} RS_1 < T_{35} \\ RS_2 < T_{35} \\ RS_{1\&2} > T_{70} \end{cases}$$

Cases in which just RS_1 or RS_2 was below threshold were not considered, since those could be nonresponding rather than contributing regions to the combined response. Combined inhibition was identified as the case in which

$$\begin{cases} RS_1 > T_{70} \\ RS_2 > T_{70} \\ RS_{1\&2} < T_{35} \end{cases}$$

For comparison, the case of single threshold crossing at T_{70} was also considered.

Since recordings are affected by noise, a lower limit for signal detection was determined by assuming that VSD maps lacked any internal structure. To simulate this condition, data matrices were generated from a uniform random distribution (MATLAB, The MathWorks) to form random maps (64×96 pixels, equivalent to MICAM01 chip size). Random numbers were scaled to match the fluorescence fluctuation recorded experimentally. Then, random maps were processed using T_{35} and T_{70} as for single- and double-threshold analysis of real data (see preceding text), thereby calculating the percentage of activated area that would be detected with a casual pattern. The amount of combined excitation and combined inhibition calculated in this way was marginal compared with that of the experimental data and was devoid of any specific time courses (Fig. 8, dashed lines), indicating that noise did not considerably affect the detection of combinatorial operations.

The extension of active areas was calculated by measuring the number of pixels crossing the T_{70} threshold of the maximum normalized response. The area variation following various treatments was measured as the relative difference between experimental conditions.

RESULTS

General properties of VSD signals

In this work we have used VSD imaging to assess the impact of double-bundle stimulation on cerebellar granular layer responses. The VSD signal generated by mossy fiber stimulation rapidly invaded the granular layer (Fig. 1A). The VSD signal was made of spots of activity grouped into clusters of irregular, often elongated shape occupying wide sectors of the granular layer. The spot diameter ($32.54 \pm 4.62 \mu\text{m}$; $n = 47$ spots, 8 slices) was estimated by setting a 70% threshold to delimit the spot contour. By using this measure to generate artificial spots at appropriate distances, mathematical simulations allowed us to reconstruct the spot/cluster structure (see Supplemental Material), suggesting that spots were indeed elementary functional units of the granular layer and that relevant combinatorial effects had to be searched at the spot level.

The origin of the VSD signal was assessed by a comparison with extracellular field potentials, which were simultaneously recorded with a multielectrode array (MEA) placed under the slice ($n = 6$; Fig. 1A; cf. Mapelli and D'Angelo 2007). The MEA had electrodes separated by $100 \mu\text{m}$, which could not reveal the spot-based structure of the granular layer response. Nonetheless, after appropriate filtering, the VSD became similar to MEA maps ($n = 6$ experiments), demonstrating that VSD and MEA were likely to

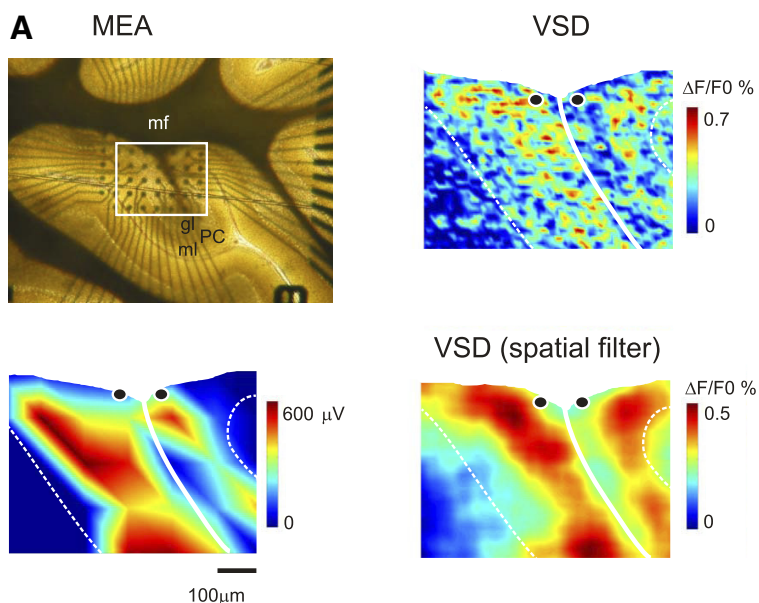
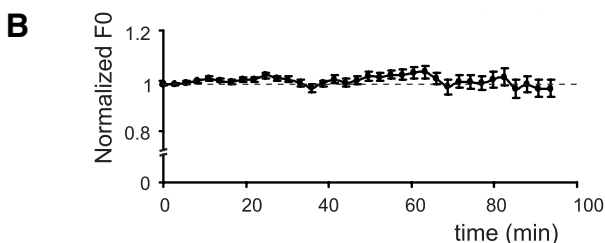


FIG. 1. The relationship between voltage-sensitive dye (VSD) and multielectrode array (MEA) signals. *A*, top left: parasagittal slice of the cerebellar vermis placed on the MEA. mf, mossy fiber; gl, granular layer; PC, Purkinje cells; ml, molecular layer. The white rectangle delimits the area detected by the camera, which is shown in the other panels. *Bottom*: MEA electrical map (see Mapelli and D'Angelo 2007). *Right, top*: optical maps of evoked granular layer activity obtained with VSD imaging. *Bottom*: same VSD recording after spatial filtering to match the MEA result. In these and the following maps, black dots indicate the pair of stimulating electrodes, dashed white lines represent the PC, and continuous white line indicates MF. *B*: time course of VSD amplitude ($\Delta F/F_0$) in a region of interest (ROI). Data are means \pm SE ($n = 10$). Note stability of the VSD signals over time.



be generated by the same signal sources. The VSD response to mossy fiber stimulation remained stable for >1 h, with a modest ($<5\%$) decay possibly caused by photobleaching (Fig. 1B).

To assess the activity state of neurons generating the VSD signal, whole cell recordings were performed from granule cells in the core of responding areas (Fig. 2A), both in the control condition ($n = 4$) and with $10 \mu\text{M}$ bicuculline ($n = 5$). The granule cells showed excitatory postsynaptic potentials (EPSPs) and EPSP–spike complexes in variable proportions, depending on the stimulation intensity (cf. D’Angelo et al. 1995). At low intensity, the VSD signal taken from the ROI surrounding the patch electrode had a shape and size reflecting that of the EPSP. At higher intensity, EPSP–spike complexes dominated the granule cell responses and the VSD response increased accordingly. However, the VSD response remained slower and proportionately smaller than the average intracellular electrical response. This was probably due to a series of factors, including the 1) limited sampling frequency of the system (typically 1 kHz), 2) the predominance of granule cells making EPSPs over those making spikes, 3) the time scattering of spikes in different cells, and 4) inhomogeneity between core and periphery of the ROI. Despite this limitation, the intensity of VSD responses in an excited area was directly proportional to the average change in intracellular membrane potential (Fig. 2B), indicating that single granule cell activity is correlated with the ensemble population signal (see Grinvald and Hildesheim 2004 for a similar observation in the neocortex). It was thus possible to identify a threshold at 70% of maximum VSD signal amplitude ideally separating subthreshold responses from spikes. This separation has to be interpreted in statistical terms, so that crossing the 70% threshold means considerably raising the probability of transiting from a nonspiking to a spiking regime in granule cell responses.

Delayed inhibition in granular layer responses

It has recently been proposed that inhibition in granule cells could be delayed with respect to mossy fiber excitation generating the so-called time-window effect (D’Angelo and DeZeeuw 2009). Since this could have an impact on combinatorial responses generated by double-bundle stimulation, the granular layer response was assessed at different times by modifying the efficiency of the principal mechanisms regulating granule cell activity—i.e., the number of active mossy fibers and the strength of the excitatory and inhibitory loops (Fig. 3).

The active area was analyzed in two neighboring time periods (0–4 and 5–9 ms), which are critical for the emergence of the window effect (Kanichay and Silver 2008; Mapelli et al. 2007). Although recruiting additional mossy fibers by increasing stimulation (D’Angelo et al. 1995; Sola et al. 2004) sorted a similar effect in these time windows ($65.1 \pm 26.5\%$ at 0–4 ms vs. $71 \pm 23.8\%$ at 5–9 ms; $P = 0.87$, $n = 4$ slices, paired t -test), differential regulation was observed by altering the excitatory/inhibitory balance. Following application of the GABA_A receptor blockers $10 \mu\text{M}$ bicuculline ($n = 10$) or $10 \mu\text{M}$ gabazine ($n = 4$), which reduce the strength of Golgi cell–granule cell connections (Mapelli et al. 2009; Fig. 3B), the extension of granular layer activity increased more in the second than in the first time period ($18.5 \pm 5.8\%$ at 0–4 ms vs. $188.7 \pm 25.2\%$ at 5–9 ms; $P < 10^{-6}$, $n = 14$ slices, paired t -test). After the first 4 ms, inhibition regulates the effectiveness of excitation mostly by controlling NMDA channel unblock and regenerative activation of the

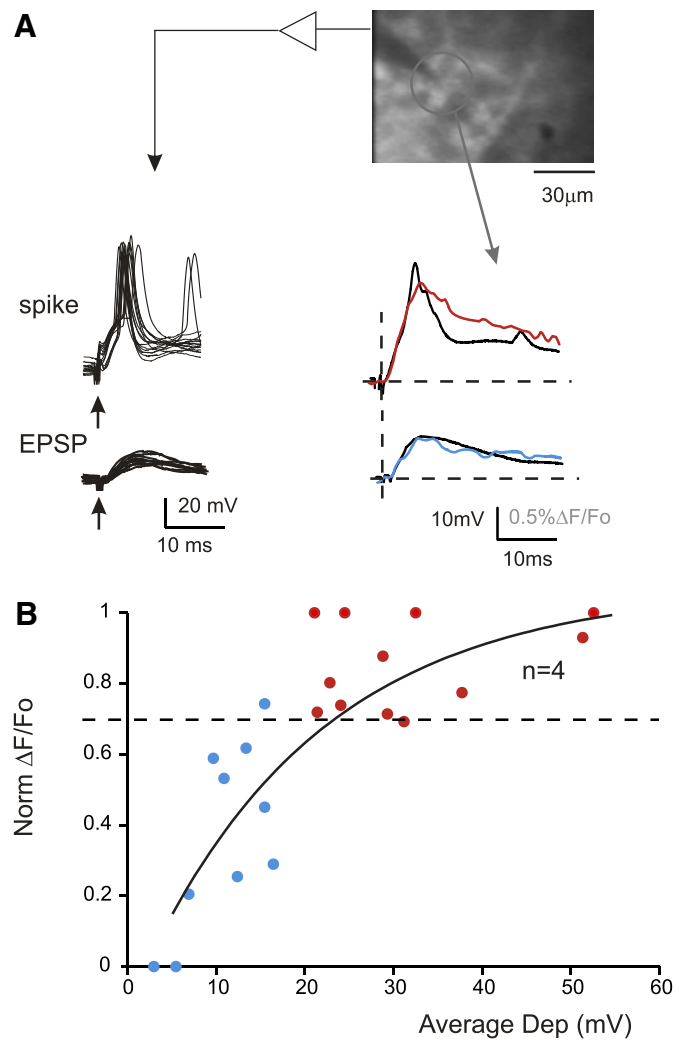


FIG. 2. The relationship between VSD signals and granule cell activity. *A*: image of a stained cerebellar slice obtained by collecting background epifluorescence showing a portion of the granular layer during a whole cell recording. Note that the patch pipette appears as a shadow since it is not filled with dye molecules. Excitatory postsynaptic potentials (EPSPs) and EPSP–spike complexes were obtained at low and high stimulation intensity, respectively. The circle indicates the ROI surrounding the recorded granule cell, from which the VSD signal has been measured. Average electrical signals (black traces) are compared with average fluorescence changes (blue and red traces). *B*: correlation between average fluorescence change and average membrane depolarization. Note that fluorescence values are normalized to maximum responses (cf. Petersen and Sakmann 2001). The dotted line corresponds to threshold set at 70% and fitting is performed with an exponential function [$y = A_1[1 - \exp(-x/\tau)]$; $A_1 = 1.06$, $\tau = 20.2$]. Red circles indicate cases in which granule cells responded with spikes in at least half of the stimulation sweeps. Data points are taken from 4 different cells (see METHODS).

NMDA current (D’Angelo et al. 1995; Mapelli et al. 2007). Accordingly, following application of the NMDA receptor antagonist $50 \mu\text{M}$ APV ($n = 4$) (Fig. 3D), the extension of granular layer activity decreased more in the second than in the first time period ($-18.7 \pm 8.7\%$ at 0–4 ms vs. $-48.3 \pm 5.1\%$ at 5–9 ms; $P < 0.01$, $n = 4$ slices, paired t -test).

The time course of changes induced by the different treatments was measured in representative areas corresponding to visually identified spots. By simply raising the stimulus intensity, the granular layer response changes observed at peak were maintained for ≥ 50 ms (53.3 ± 14.6 vs. $46.7 \pm 9.9\%$, $n = 4$, $P <$

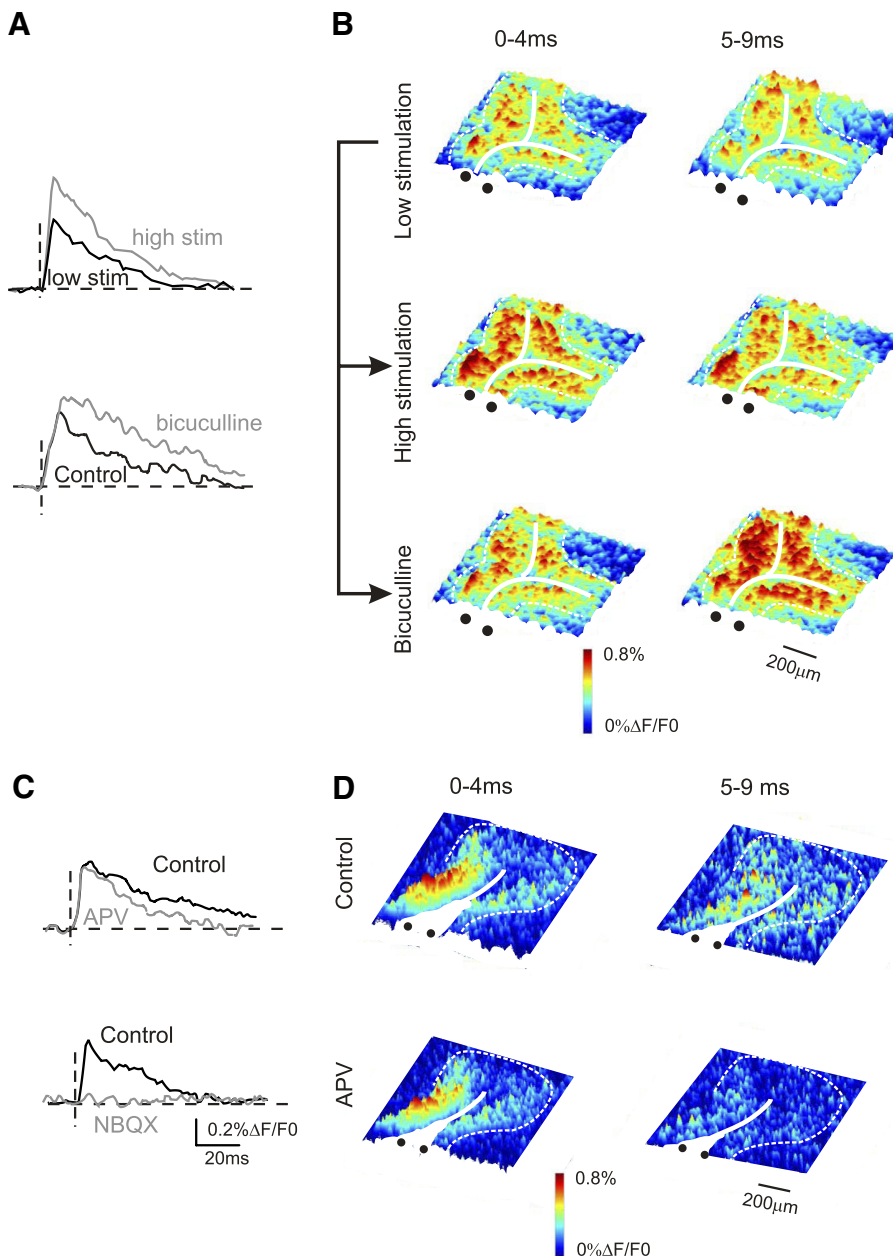


FIG. 3. The impact of GABA and NMDA receptors on granular layer responses. *A*: the VSD signal was enhanced by increasing the stimulation intensity and by the GABA_A receptor blocker, 10 μ M bicuculline. Note that the GABA receptors were most effective in the late component of the response. *B*: VSD maps of granular activity obtained in response to mossy fiber stimulation at 2 different intensities (3 and 7 V) and after application of 10 μ M bicuculline. The maps are shown during the first 0–4 ms, when only excitation is present, and at 5–9 ms, when feedforward inhibition is activated. Note that, whereas the response enhancement caused by increased stimulation is already evident at 0–4 ms and persists thereafter, that caused by bicuculline is delayed and appears at 5–9 ms. *C*: the VSD signal was reduced by the NMDA receptor blocker, 50 μ M APV, whereas the AMPA receptor blocker, 10 μ M NBQX, completely suppressed the response. *D*: VSD maps of granular activity obtained in response to mossy fiber stimulation and after the application of 50 μ M APV. The maps are shown at the peak of the response and at 5–9 ms after the stimulus, when the effect of the block NMDA receptors is most evident. Note that the reduction of granular layer activity is most evident in the late phase of the response. *D*: VSD maps of granular activity obtained in response to mossy fiber stimulation and after the application of 50 μ M APV. The maps are shown at the peak of the response and at 5–9 ms after the stimulus, when the effect of the block NMDA receptors is most evident. Note that the reduction of granular layer activity is most evident in the late phase of the response. GABA, γ -aminobutyric acid; NMDA, *N*-methyl-D-aspartate; AMPA, α -amino-3-hydroxy-5-methyl-4-isoxazolepropionic acid; NBQX, 2,3-dihydroxy-6-nitro-7-sulfamoyl-benzo[f]quinoxaline-2,3-dione; D-APV, 2-amino-5-phosphonovaleic acid.

0.64, paired *t*-test; Fig. 3A). However, application of 10 μ M bicuculline or 10 μ M gabazine ($n = 4$) caused a much smaller signal increase at peak than after 50 ms (32.2 ± 5.1 vs. $123.9 \pm 33.4\%$; $n = 14$ experiments; $P < 0.01$, paired *t*-test; Fig. 3A). Consistently, application of 50 μ M APV caused a much smaller signal decrease at peak than after 50 ms (-28.1 ± 6.9 vs. $-57 \pm 11.1\%$; $n = 4$, $P < 0.01$, paired *t*-test; Fig. 3C).

Therefore the action of inhibition arose with a delay of about 5 ms and persisted for ≥ 50 ms. The excitatory/inhibitory balance in this delayed period of the response was regulated by GABA_A (inhibitory) and NMDA (excitatory) receptors. Any responses were finally suppressed by 10 μ M NBQX (Fig. 3C), indicating that AMPA receptors provided the necessary depolarization triggering the response. These observations indicate that the general mechanism of regulation of the granular layer response (Armano et al. 2000; Mapelli and D'Angelo 2007; for review see D'Angelo and DeZeeuw 2009) can be observed using VSD imaging.

Double-bundle stimulation reveals combinatorial operations in the granular layer

The structural organization of the cerebellum granular layer suggests that it should be able to perform combinatorial operations on incoming mossy fiber inputs. On the one hand, combined excitation generated by convergent inputs could enhance activation in specific granule cell subsets. On the other hand, the Golgi cells converging through lateral connections onto some granule cell subsets could generate combined inhibition. These effects have been predicted to generate, as computational counterpart, coincidence detection and spatial pattern separation (Albus 1971; Fujita 1982; Marr 1969).

Figure 4A shows a typical double-bundle experiment. As a whole, the overlapping area was more excited when the two bundles were activated together rather than independently (the increase was $42.7 \pm 12.4\%$; $n = 12$ slices; $P < 0.05$, paired *t*-test;

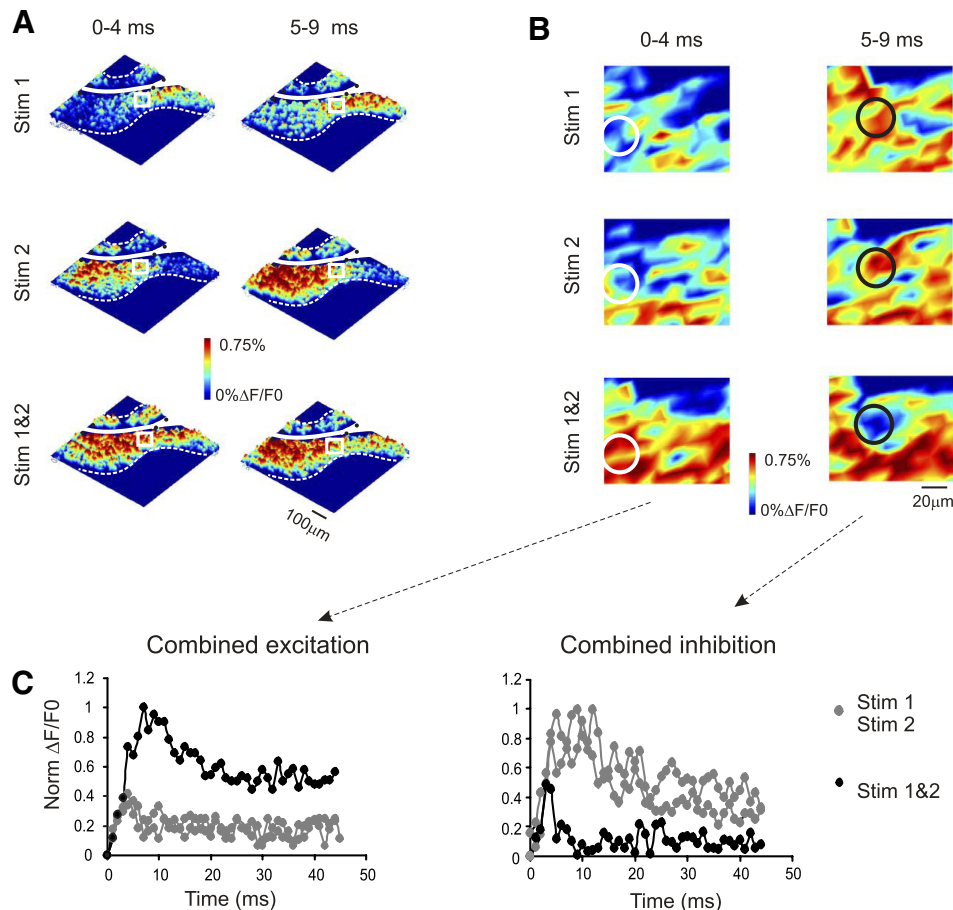


FIG. 4. Combined excitation and combined inhibition on double-bundle stimulation. **A:** VSD maps were obtained by stimulating independently (Stim1, Stim2) or simultaneously (Stim1&2) 2 separate portions of the mossy fiber bundle with different couples of MEA electrodes (black dots). The response is shown in 2 time windows (0–4 and 5–9 ms after the stimuli). Visual inspection of these large-scale maps evidences spatial summation as the major effect of double-bundle stimulation. **B:** a detailed view (taken inside the white box drawn in **A**) reveals a more complex organization of the response. White circles indicate a region in which the conjoint response is enhanced compared with single responses at 0–4 ms. Black circles indicate a region in which the conjoint response is cancelled at 5–9 ms. **C:** the time courses of VSD signal relative to the patterns shown in **B**. Gray dots correspond to responses to single-bundle stimulation; black dots correspond to responses to double-bundle stimulation. Note that the 2 ROIs identified in **B** show quite different responses, designated as combined excitation (corresponding to **B**, left) and combined inhibition (corresponding to **B**, right). Clearly, combined excitation showed immediate and persistent enhancement in the double response, whereas combined inhibition showed a delayed reduction in the combined response.

Fig. 4A). This was not unexpected given the effect of mossy fiber recruitment reported in Fig. 3 (see also D'Angelo et al. 1995; Sola et al. 2004). However, fine-grain analysis evidenced a more complex pattern on the spot scale (Fig. 4B). Whereas in some areas the response was enhanced by double-bundle stimulation (combined excitation), in others the opposite occurred so that the response was strongly reduced (combined inhibition) (Fig. 4B).

The analysis performed on visually selected spots showed that, in the case of combined excitation, the time course of the combined response rapidly increased during the first 5 ms and maintained a sustained level for the subsequent 20 ms (Fig. 4C, left). This was likely to reflect rapid EPSP temporal summation and spike generation in granule cells, which are known to respond within 2–4 ms from the stimulus (D'Angelo 2008; D'Angelo et al. 1999; Jörntell and Ekerot 2006). In the case of combined inhibition (Fig. 4C, right), the combined response also peaked in about 5 ms but then rapidly declined below the level of individual responses.

The average response in several spots showed a time course similar to that in individual spots, indicating that the two patterns were indeed typical and reproducible (Fig. 5A). The analysis of combinatorial operations was extended by investigating their time course during repetitive stimulation (Fig. 5, B and C), which represents the common mode of mossy fiber discharge (Chaderton et al. 2004; Jörntell and Ekerot 2006; Kase et al. 1980; Prsa et al. 2009; Rancz et al. 2007; van Kan et al. 1993, 1994). In response to bursts composed of five impulses at either 100 or 500 Hz, granular layer activation became more intense and reliable (this is clearly visible in the insets to Fig. 5 and in the movies reported in the Supplemental Material). The differential behavior

of spots performing combined excitation or combined inhibition was also observed in these cases. In particular, combined excitation was manifest as a persistent enhancement of the combined response during and after stimulation, whereas combined inhibition was characterized by an initial growth followed by a marked decline of the combined response just after the end of the stimulus train (cf. Fig. 5, B and C).

The ability of neurons to making spikes implies sharp nonlinear transitions in the intensity of responses. With combined excitation the combined response to single stimuli was significantly larger than the sum of the individual responses (by $47.6 \pm 8.9\%$; $n = 25$ ROI, $n = 5$ slices, $P < 0.001$, paired t -test), whereas with combined inhibition the combined response was smaller than the sum of the individual responses (by $-85.4 \pm 1.6\%$; $n = 25$ ROI, $n = 5$ slices, $P < 0.001$, paired t -test) and usually even of individual responses themselves. Similarly significant statistics were observed for responses to train stimulation, as shown in Fig. 5 (inset histograms). Thus combined excitation and combined inhibition are compatible with the concepts of coincidence detection and spatial pattern separation predicted by theory (Albus 1971; Fujita 1982; Marr 1969).

Stability, time course, and extension of combinatorial responses

A quantification of the extension of combinatorial operations was obtained by measuring the granular layer activity changes across a double (T_{35} – T_{70}) threshold (cf. Fig. 2B and METHODS). This generated an ideal separation between high- and low-probability spiking areas and allowed us to detect the combi-

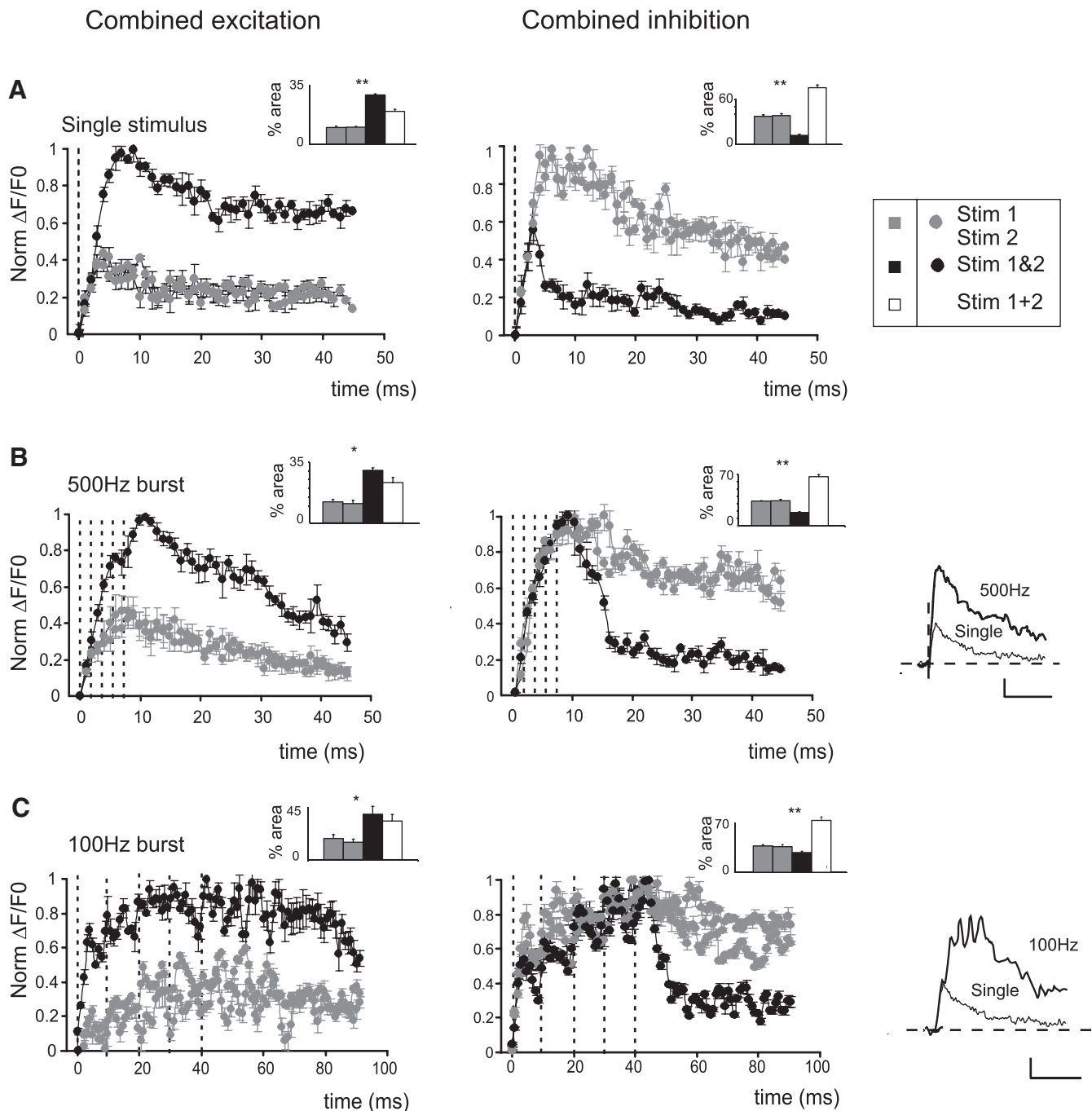


FIG. 5. Combinatorial responses elicited by repetitive stimulation. Average time course of VSD signals taken from the ROIs ($27 \times 27 \mu\text{m}^2$) showing similar patterns of activation (either combined excitation or combined inhibition) in response to the stimulation of mossy fibers (A) with a single pulse ($n = 5$), (B) with a 500-Hz burst ($n = 5$), and (C) with a 100-Hz burst ($n = 5$). *Left*: average time course of VSD signals showing combined excitation. *Right*: average time course of VSD signal showing combined inhibition. The plots show single-bundle stimulation (gray dots) and double-bundle stimulation (black dots) and dashed lines indicate the stimulus times. Note that, with all patterns, the double-bundle response is enhanced in ROIs performing combined excitation, but is reduced in ROIs performing combined inhibition. The *insets* show the VSD signals generated by 500- and 100-Hz bursts compared with single-pulse stimulation (scale bars $0.2\% \Delta F/F_0$, 50 ms). The histograms show % peak change, demonstrating supralinear increase during combined excitation and reduction during combined inhibition ($P < 0.01$ between A + B and A&B in all the experimental conditions, paired *t*-test).

natorial operations automatically without the intervention of subjective spot selection and to efficiently extend analysis over all detectable spots in all the available experiments. Clustered groups of pixels showed characteristic spatiotemporal evolution of the combinatorial operations (Fig. 6, A and B). During the 20–25 ms following the stimulus, the extension and intensity of responses evolved following slightly different time

courses in the individual clusters (Fig. 6, A and B). Combined inhibition often showed oscillations that could correspond to reverberation of inhibition through local circuit loops (see DISCUSSION). Similar results were obtained using single stimuli as well as bursts at 100 and 500 Hz (data not shown).

Combined excitation and combined inhibition occupied, as a proportion of the commonly activated area, respectively,

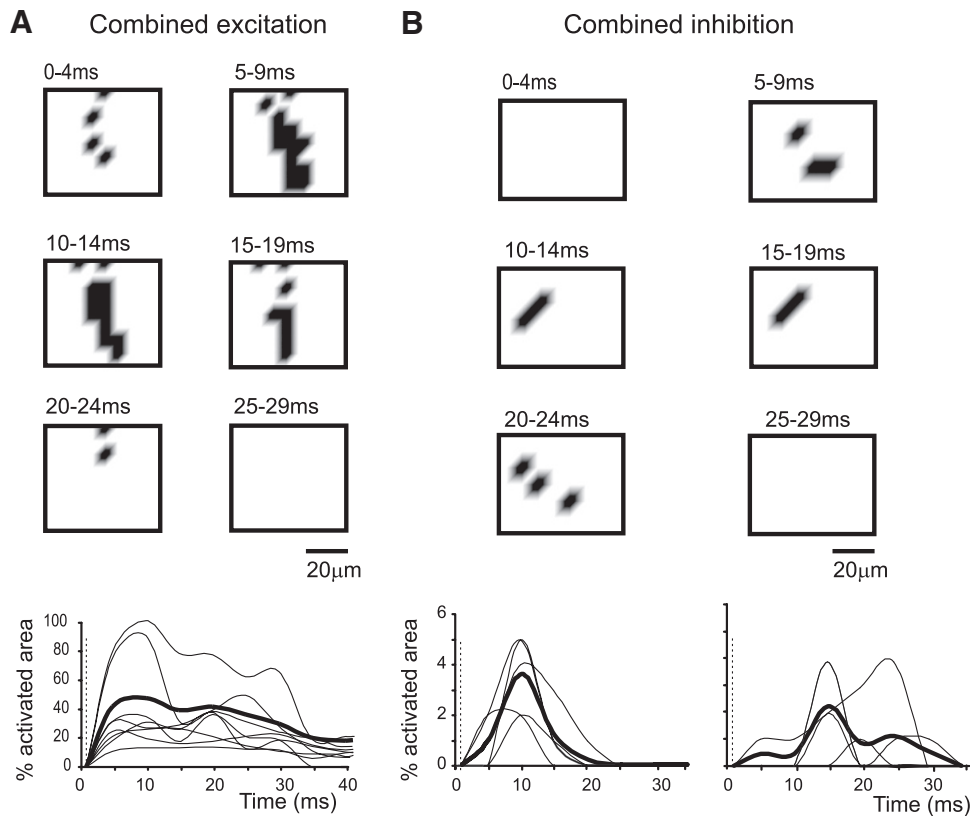


FIG. 6. Local stability and evolution of combinatorial responses. *A*, top: pixels performing combined excitation at different timeframes and the graph shows the time courses of several such pixels. Data collected from different experiments are indicated by gray lines and the ensemble behavior is indicated with a thick black line ($n = 9$). Combined excitation shows an early activation, reaches its maximum in a few milliseconds (5–10), and then slowly decreases. *B*, top: pixels performing combined inhibition at different timeframes and the graphs show the time courses of several such pixels. Data collected from different experiments are indicated by gray lines and the ensemble behaviors are indicated with thick black lines ($n = 9$). In the majority of cases, combined inhibition shows a delayed activation, reaches its maximum beyond 10 ms, and slowly decreases (*left*; $n = 5$). In some cases combined inhibition shows rebound phases at 20–25 ms, probably due to some feedback loops (*right*; $n = 4$). Traces in the 2 panels have been sorted according to increasingly delayed activation.

45.2 ± 8.7 and $2.04 \pm 0.54\%$ with single stimuli ($n = 10$ slices), 49.35 ± 10.34 and $3.44 \pm 1.4\%$ with 500-Hz bursts ($n = 5$ slices), and 51.96 ± 11.8 and $3.65 \pm 1.35\%$ with 100-Hz bursts ($n = 10$ slices). It should be noted that, by adopting a single T_{70} threshold criterion, combined excitation marginally increased, whereas combined inhibition increased up to around 15% of the commonly activated area, suggesting that this latter process was especially underestimated in our analysis. Nonetheless, in general, regions performing combined inhibition were less extended than those performing combined excitation (cf. Figs. 4 and 7).

Regulation of spatiotemporal dynamics by repetitive stimulation and synaptic inhibition

The maps reported in Fig. 7 show the distribution of areas performing combined excitation and combined inhibition. With all stimulus patterns, combined inhibition was scattered in several spots over the activated area in common to the two stimuli. The average time course of combinatorial operations averaged over all the spots in the same category is shown in Fig. 8. With all stimulus patterns, combined excitation arose rapidly and progressively declined after the stimuli. Conversely, combined inhibition was almost absent during stimulation but arose soon thereafter.

The delayed occurrence of combined inhibition suggested that it was dynamically regulated by synaptic inhibitory loops, which in the granular layer can provide both delayed activation and lateral inhibition (D'Angelo and DeZeeuw 2009; D'Angelo et al. 2009). To test this hypothesis, double-bundle stimulation experiments were continued with the application of $10 \mu\text{M}$ bicuculline to block GABAergic transmission

from Golgi to granule cells. After application of bicuculline, combined inhibition was almost entirely abolished, whereas combined excitation increased (Figs. 7 and 8). With single stimuli, the change induced by bicuculline in combined inhibition was maximal at 10–20 ms ($-95.1 \pm 4.9\%$; $n = 12$, $P < 0.001$, paired t -test). Significant differences were also induced by bicuculline using repetitive stimulation, with maximum significant changes in combined inhibition occurring 20–40 ms after the end of 500-Hz bursts (-100% , $n = 5$, $P < 0.0001$, paired t -test) and 50–80 ms after the end of 100-Hz bursts ($-65.5 \pm 11.4\%$, $n = 11$, $P < 0.01$, paired t -test). In the same time periods, there were also significant changes in coincidence detection but in the opposite direction (single stimuli, $55.87 \pm 5.9\%$; $n = 12$, $P < 0.01$; 500-Hz bursts, 104.3 ± 7.9 , $n = 5$, $P < 0.01$; 500-Hz bursts, 56.3 ± 10.4 , $n = 11$, $P < 0.02$, paired t -test). This result supports the important role of synaptic inhibition to modulate combinatorial operations in the granular layer.

DISCUSSION

The central observation in this study is that the cerebellum granular layer can perform two combinatorial operations—combined excitation and combined inhibition—controlled by the relative intensity of synaptic inhibition. The combinatorial effects lasted for tens of milliseconds and combined inhibition occurred in specific granule cell subsets only after stimulation was terminated. Combined excitation and combined inhibition provide the first demonstration that combinatorial operations compatible with those predicted by theory, coincidence detection and spatial pattern separation (Albus 1971; Marr 1969), could actually take place in the cerebellum granular layer.

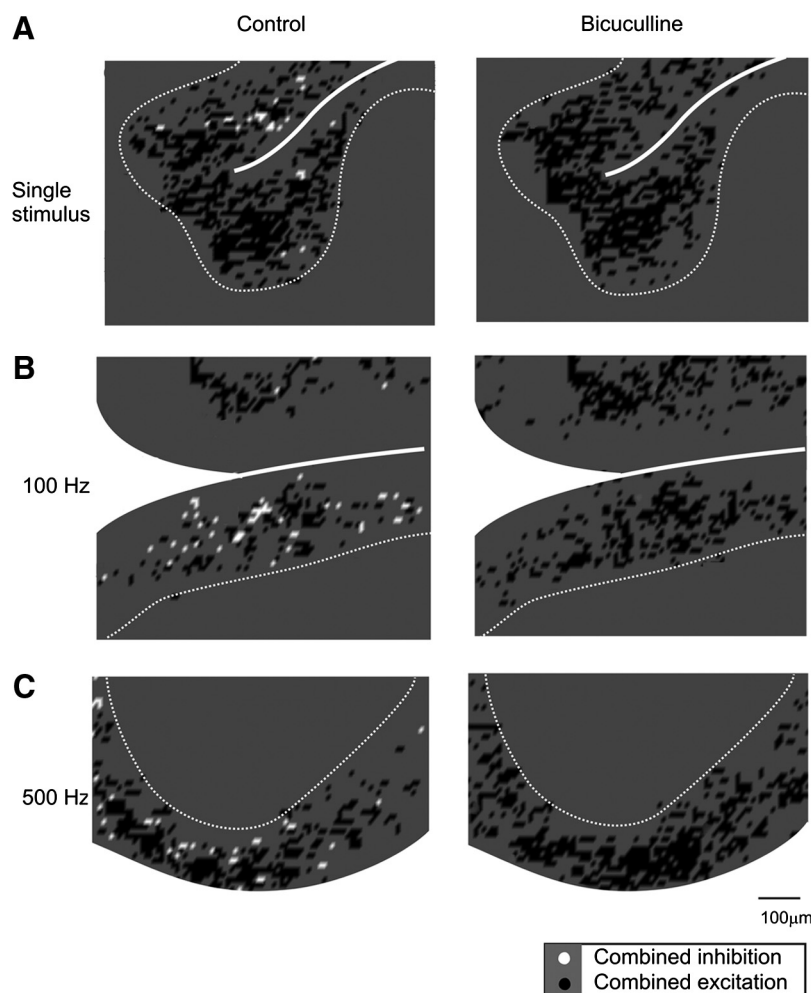


FIG. 7. The spatial organization of combinatorial responses: dependence on synaptic inhibition. *Left*: pixels performing combined inhibition (white) are scattered among pixels performing combined excitation (black) in response to the stimulation of mossy fibers (*A*) with a single pulse, (*B*) with a 100-Hz burst, and (*C*) with a 500-Hz burst. The data were taken when combined inhibition was maximal (10 ms from the stimulus in *A*, 20 ms from the end of the burst in *B*, 50 ms from the end of the burst in *C*). *Right*: application of 10 μM bicuculline abolished combined inhibition.

The key role of local circuit inhibition for determining granular layer combinatorial operations was supported by several observations. First, in combined inhibition elicited by single mossy fiber pulses, the 4- to 5-ms delay coincides with the time required to enable mossy fiber \rightarrow Golgi cell \rightarrow granule cell feedforward inhibition (Barmack and Yakhnitsa 2008; Kanichay and Silver 2008; for review see D'Angelo 2008). The oscillatory responses observed in certain areas are reminiscent of similar effects generated by recurrent activity in the granule cell \rightarrow Golgi cell \rightarrow granule cell feedback inhibitory loop (e.g., see Maex and DeSchutter 1998). Second, inhibition revealed a differential control over the two operations, in that combined excitation was enhanced, whereas combined inhibition was abolished by blocking GABA_A receptors. The multifunctional inhibition-dependent dynamics shown by network responses are in keeping with predictions generated by large-scale models of the granular layer (Medina and Mauk 2000; S. Solinas and E. D'Angelo, unpublished observations).

The spatial properties of ensemble granular layer activity revealed details on a scale one order of magnitude smaller than previously reported using extracellular field recordings (Mapelli and D'Angelo 2007; Morissette and Bower 1996; Shambes et al. 1978;). The combinatorial operations were manifest in small cell aggregates (called spots), with an apparent diameter around 30 μm . The size of the spots is in matching with "granular layer units" determined by branching

of mossy fibers, which form clusters of rosettes in the sagittal plane (Eccles et al. 1967; Sultan 2001; Sultan and Heck 2003). The occurrence of combinatorial operations in multiple scattered areas suggests specific local circuit topologies. In areas showing combined excitation, mossy fiber convergence onto granule cells needs to be predominant (D'Angelo et al. 1995; Jörntell and Ekerot 2006) over convergence onto Golgi cells, so that Golgi cells can only proportionately reduce granule cell activation. Conversely, in areas showing combined inhibition, the convergence of mossy fibers onto Golgi cells needs to be predominant over convergence onto granule cells, so that Golgi cells can generate effective and strong inhibition during double-bundle stimulation. It is likely that these effects require lateral inhibition (for a general discussion see Buzsáki 2006), which has indeed been reported in the cerebellum granular layer (Mapelli and D'Angelo 2007).

The kinetics of combinatorial operations also suggest the involvement of specific cellular and circuit properties. During high-frequency bursts, the granular layer response increased without being blocked by inhibition. This effect indicates that Golgi cell activity does not usually prevail over mossy fiber excitation during the burst, in line with the observation of protracted granule cell firing in response to sensory stimuli (Chadderton et al. 2004; Jörntell and Ekerot 2006; Rancz et al. 2007). The marked adaptation characterizing Golgi cell discharge (Solinas et al. 2007a,b) and the presynaptic inhibition of

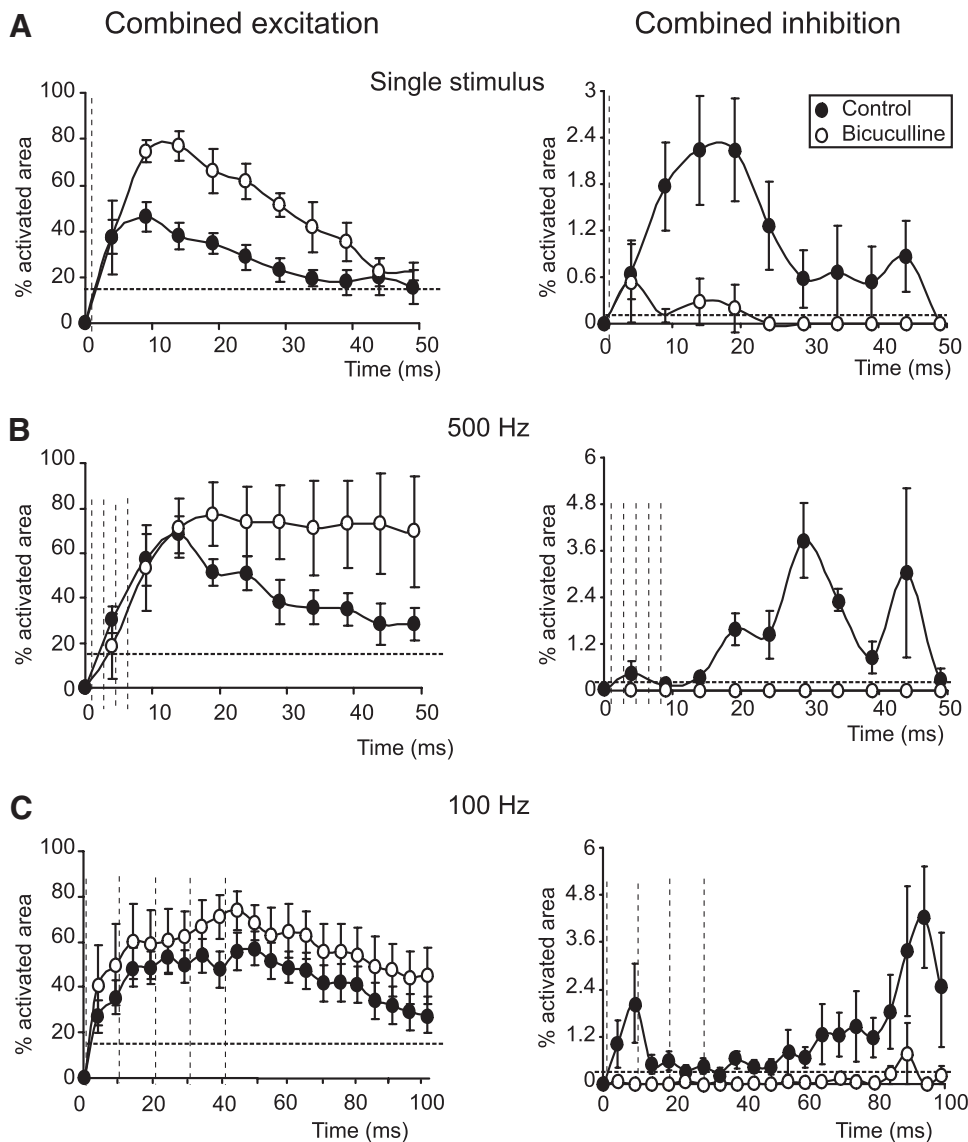


FIG. 8. The kinetics of combinatorial responses: dependence on synaptic inhibition. Time course of areas (expressed as % of commonly activated pixels) performing combined excitation and combined inhibition in control (filled circles) and in the presence of $10 \mu\text{M}$ bicuculline (open circles). *Left*: average time course of combined excitation. *Right*: average time course of combined inhibition. Responses to the stimulation of mossy fibers (A) with a single pulse ($n = 12$), (B) with a 500-Hz burst ($n = 5$), and (C) with a 100-Hz burst ($n = 11$). Note that, in all cases, combined excitation grows rapidly and then slowly decays after the end of the stimuli. Conversely, combined inhibition increases only after the end of the stimuli. Moreover, combined excitation is enhanced by $10 \mu\text{M}$ bicuculline application while combined inhibition is abolished. In all panels dashed horizontal lines indicate the average amount of combined excitation and combined inhibition calculated on random matrices (see METHODS).

GABA release through metabotropic glutamate and GABA_B receptors (Mapelli et al. 2009; Mitchell and Silver 2003) could decrease the efficiency of granule cell inhibition during the burst. Second, after termination of the stimulus, the presence of delayed responses implies that granule cell excitation is protracted and that inhibition can strongly interfere with this late response. This effect is likely to reflect the interplay of the NMDA receptor-mediated conductance, which generates an afterdepolarization lasting for as long as 100 ms (see Fig. 2A; D'Angelo et al. 1995), and the GABA receptor-mediated conductance, which can also last for a similar time (see Fig. 2A; Eccles et al. 1967; Maffei et al. 2002) due to spillover-mediated activation of $\alpha 6$ receptors (Rossi and Haman 2003). Actually, the NMDA current is weakly regenerative and its depolarizing effect can be effectively turned off by raising the granule cell input conductance through GABA_A receptor opening (Mapelli and D'Angelo 2007).

Combined excitation and combined inhibition may be regulated by several factors determining the excitatory/inhibitory balance of granule cells *in vivo*. The intensity and distribution of the mossy fiber inputs, the partially independent control of

granule and Golgi cells from different receptive fields (Jörntell and Ekerot 2002), and the block of Golgi cell activity by stellate cells (but perhaps also by Purkinje cells and Lugaro cells: Barmack and Yakhnitsa 2008; for review see D'Angelo 2008) leave ample space for the spatiotemporal organization of combinatorial operators. Moreover, synaptic plasticity in granular layer circuit synapses may generate new configurations by controlling the local excitatory/inhibitory balance (D'Angelo and DeZeeuw 2009; Hansel et al. 2001; Mapelli and D'Angelo 2007). Finally, it should be noted that the effectiveness of inhibition, and therefore of combined inhibition, may be larger in the intact tissue than that in the present experiments, since connections made by laterally oriented Golgi cell axons are severed at the slice border. It follows that the major role of the Golgi cells may indeed be that of generating surround inhibition implementing spatial pattern separation rather than performing gain control over mossy fiber inputs (cf. Prsa et al. 2009).

Combined excitation and combined inhibition are likely to represent the counterpart of coincidence detection and spatial pattern separation defined in Motor Learning Theory (Albus

1971; Gibson et al. 1991; Marr 1969, 1971; Torioka 1980; Tyrrell and Willshaw 1992) and may therefore bear several implications for cerebellar circuit functioning. Coincidence detection and spatial pattern separation may contribute to generate the output spike patterns to be relayed to Purkinje cells (D'Angelo and DeZeeuw 2009; Pouille et al. 2001). In that the properties observed in vitro are exploited by natural patterns in vivo (e.g., see Prsa et al. 2009; van Kan 1993, 1994), spatial pattern separation may be particularly relevant to processing sequences of bursts rather than individual bursts, preventing certain granular cell groups from being reactivated by a second input occurring within some tens of milliseconds. Thus the long-sought spatiotemporal filtering predicted by theory (Fujita 1982) may work as a device regulating cycles of circuit reactivation in center-surround geometry. This in turn would promote selection of Purkinje cells (Brunel et al. 2004; de Solages et al. 2008; Steuber et al. 2007) during presentation of complex spatiotemporal mossy fiber patterns. It should also be noted that the present circuit mechanism may implement logical operations (including "Exclusive OR" [XOR]; Churchland and Sejnowski 1992), an aspect deserving further experimental and theoretical analysis.

ACKNOWLEDGMENTS

We thank Dr. S. Fusi and Dr. L. Sacconi for critical comments on an early version of the manuscript and G. Ferrari for technical support.

GRANTS

This work was supported by a National Consortium for the Physics of Matter NEUROIMAGE grant and European Union Grant SENSOPAC FP6-IST028056. D. Gandolfi is a recipient of a Projects of National Interest fellowship of the Italian Ministry for Education, University, and Research.

REFERENCES

- Albus JS.** A theory of cerebellar function. *Math Biosci* 10: 25–61, 1971.
- Armano S, Rossi P, Taglietti V, D'Angelo E.** Long-term potentiation of intrinsic excitability at the mossy fibre: granule cell synapse of rat cerebellum. *J Neurosci* 20: 5208–5216, 2000.
- Bakker A, Kirwan CB, Miller M, Stark CE.** Spatial pattern separation in the human hippocampal CA3 and dentate gyrus. *Science* 319: 1640–1642, 2008.
- Barmack NH, Yakhnitsa V.** Functions of interneurons in mouse cerebellum. *J Neurosci* 28: 1140–1152, 2008.
- Berger T, Borgdorff A, Crochet S, Neubauer FB, Lefort S, Fauvet B, Ferezou I, Carleton A, Lüscher HR, Petersen CCH.** Combined voltage and calcium epifluorescence imaging in vitro and in vivo reveals subthreshold and suprathreshold dynamics of mouse barrel cortex. *J Neurophysiol* 97: 3751–3762, 2007.
- Brecht M, Fee MF, Garaschuk O, Helmchen F, Margrie TW, Svoboda K, Osten P.** Novel approaches to monitor and manipulate single neurons in vivo. *J Neurosci* 24: 9223–9227, 2004.
- Brunel N, Hakim V, Isope P, Nadal JP, Barbour B.** Optimal information storage and the distribution of synaptic weights: perceptron versus Purkinje cell. *Neuron* 43: 745–757, 2004.
- Buzsáki G.** Large-scale recording of neuronal ensembles. *Nat Neurosci* 7: 446–451, 2004.
- Buzsáki G.** *Rhythms of the Brain*. Oxford, UK: Oxford Univ. Press, 2006, p. 65.
- Chadderton P, Margrie TW, Hausser M.** Integration of quanta in cerebellar granule cells during sensory processing. *Nature* 428: 856–860, 2004.
- Chen G, Gao W, Reinert KC, Popa LS, Hendrix CM, Ross ME, Ebner TJ.** Involvement of kv1 potassium channels in spreading acidification and depression in the cerebellar cortex. *J Neurophysiol* 94: 1287–1298, 2005.
- Churchland P, Sejnowski TJ.** *The Computational Brain*. Cambridge, MA: The MIT Press, 1992.
- Cohen D, Yarom Y.** Patches of synchronized activity in the cerebellar cortex evoked by mossy-fiber stimulation: questioning the role of parallel fibers. *Proc Natl Acad Sci USA* 95: 15032–15036, 1998.
- Contreras D, Llinás R.** Voltage-sensitive dye imaging of neocortical spatio-temporal dynamics to afferent activation frequency. *J Neurosci* 21: 9403–9413, 2001.
- D'Angelo E.** The critical role of Golgi cells in regulating spatiotemporal integration and plasticity at the cerebellum input stage. *Front Neurosci* 2: 35–46, 2008.
- D'Angelo E, De Filippi G, Rossi P, Taglietti V.** Synaptic excitation of individual rat cerebellar granule cells in situ: evidence for the role of NMDA receptors. *J Physiol* 484: 397–413, 1995.
- D'Angelo E, DeZeeuw C.** Timing and plasticity in the cerebellum: focus on the granular layer. *Trends Neurosci* 32: 30–40, 2009.
- D'Angelo E, Nieuw T, Maffei A, Armano S, Rossi P, Taglietti V, Fontana A, Naldi G.** Theta-frequency bursting and resonance in cerebellar granule cells: experimental evidence and modeling of a slow K⁺-dependent mechanism. *J Neurosci* 21: 759–770, 2001.
- D'Angelo E, Rossi P, Armano S, Taglietti V.** Evidence for NMDA and mGlu receptor-dependent long-term potentiation of mossy fiber-granule cell transmission in rat cerebellum. *J Neurophysiol* 81: 277–287, 1999.
- Derdikman D, Hildesheim R, Ahissar E, Arieli A, Grinvald A.** Imaging spatiotemporal dynamics of surround inhibition in the barrels somatosensory cortex. *J Neurosci* 23: 3100–3105, 2003.
- de Solages C, Szapiro G, Brunel N, Hakim V, Isope P, Buisseret P, Rousseau C, Barbour B, Léna C.** High-frequency organization and synchrony of activity in the Purkinje cell layer of the cerebellum. *Neuron* 58: 775–788, 2008.
- Dieudonné S.** Submillisecond kinetics and low efficacy of parallel fiber-Golgi cell synaptic currents in the rat cerebellum. *J Physiol* 510: 845–866, 1998.
- Dugué GP, Dumoulin A, Triller A, Dieudonné S.** Target-dependent use of co-released inhibitory transmitters at central synapses. *J Neurosci* 25: 6490–6498, 2005.
- Ebner TJ, Chen G, Gao W, Reinert K.** Optical imaging of cerebellar functional architectures: parallel fiber beams, parasagittal bands and spreading acidification. *Prog Brain Res* 148: 125–138, 2005.
- Eccles JC, Ito M, Szentagothai J.** *The Cerebellum as a Neuronal Machine*. Berlin: Springer-Verlag, 1967.
- Elias SA, Yae H, Ebner TJ.** Optical imaging of parallel fiber activation in the rat cerebellar cortex: spatial effects of excitatory amino acids. *Neuroscience* 52: 771–786, 1993.
- Ferezou I, Bolea S, Petersen CCH.** Visualizing the cortical representation of whisker touch: voltage-sensitive dye imaging in freely moving mice. *Neuron* 50: 617–629, 2006.
- Fujita M.** Adaptive filter model of the cerebellum. *Biol Cybern* 45: 195–206, 1982.
- Fyhn M, Hafting T, Treves A, Moser MB, Moser EI.** Hippocampal remapping and grid realignment in entorhinal cortex. *Nature* 446: 190–194, 2007.
- Galvan EJ, Clisto E, Barrionuevo G.** Bidirectional Hebbian plasticity at hippocampal mossy fiber synapses on CA3 interneurons. *J Neurosci* 28: 14042–14055, 2008.
- Gibson WG, Robinson J, Bennett MR.** Probabilistic secretion of quanta in the central nervous system: granule cell synaptic control of spatial pattern separation and activity regulation. *Philos Trans R Soc Lond B Biol Sci* 332: 199–220, 1991.
- Grinvald A, Hildesheim R.** VSFI: a new era in functional imaging of cortical dynamics. *Nat Rev Neurosci* 5: 874–875, 2004.
- Hansel C, Linden DJ, D'Angelo E.** Beyond parallel fiber LTD: the diversity of synaptic and non-synaptic plasticity in the cerebellum. *Nat Neurosci* 4: 467–475, 2001.
- Harvey RJ, Napper RM.** Quantitative studies on the mammalian cerebellum. *Prog Neurobiol* 36: 437–467, 1991.
- Jörntell H, Ekerot CF.** Reciprocal bidirectional plasticity of parallel fiber receptive fields in cerebellar Purkinje cells and their afferent interneurons. *Neuron* 34: 797–806, 2002.
- Jörntell H, Ekerot CF.** Properties of somatosensory synaptic integration in cerebellar granule cells in vivo. *J Neurosci* 26: 11786–11797, 2006.
- Kanichay RT, Silver RA.** Synaptic and cellular properties of the feedforward inhibitory circuit within the input layer of the cerebellar cortex. *J Neurosci* 28: 8955–8967, 2008.
- Kase M, Miller DC, Noda H.** Discharges of Purkinje cells and mossy fibres in the cerebellar vermis of the monkey during saccadic eye movements and fixation. *J Physiol* 300: 445–453, 1980.
- Leutgeb JK, Leutgeb S, Moser MB, Moser EI.** Spatial pattern separation in the dentate gyrus and CA3 of the hippocampus. *Science* 16: 961–966, 2007.

- Maex R, De Schutter E.** Synchronization of Golgi and granule cell firing in a detailed network model of the cerebellar granule cell layer. *J Neurophysiol* 80: 2521–2537, 1998.
- Mapelli J, D'Angelo E.** The spatial organization of long-term synaptic plasticity at the input stage of the cerebellum. *J Neurosci* 27: 1285–1296, 2007.
- Mapelli L, Rossi P, Nieuws T, D'Angelo E.** Tonic activation of GABA-B receptors reduces release probability at inhibitory connections in the cerebellar glomerulus. *J Neurophysiol* 101: 3089–3099, 2009.
- Marr DA.** Theory of the cerebellar cortex. *J Physiol* 202: 437–470, 1969.
- Marr DA.** Simple memory: a theory for archicortex. *Philos Trans R Soc Lond B Biol Sci* 262: 23–81, 1971.
- McNaughton BL, Nadel L.** Hebb–Marr networks and the neurobiological representation of action in space. In: *Neuroscience and Connectionist Theory*, edited by Gluck MA, Rumelhart DE. Hillsdale, NJ: Erlbaum, 1989, p. 1–63.
- Medina JF, Mauk MD.** Computer simulation of cerebellar information processing. *Nat Neurosci Rev* 3: 1205–1211, 2000.
- Mitchell SJ, Silver RA.** Shunting inhibition modulates neuronal gain during synaptic excitation. *Neuron* 38: 433–445, 2003.
- Morissette J, Bower JM.** Contribution of somatosensory cortex to responses in the rat cerebellar granule cell layer following peripheral tactile stimulation. *Exp Brain Res* 109: 240–250, 1996.
- Nicolelis MA, Dimitrov D, Carmena JM, Crist R, Lehew G, Kralik JD, Wise SP.** Chronic, multisite, multielectrode recordings in macaque monkeys. *Proc Natl Acad Sci USA* 100: 11041–11046, 2003.
- Nieuws T, Sola E, Mapelli J, Saftenku E, Rossi P, D'Angelo E.** LTP regulates burst initiation and frequency at mossy-fiber-granule cell synapses of rat cerebellum: experimental observations and theoretical predictions. *J Neurophysiol* 95: 686–699, 2006.
- Petersen CCH, Sakmann B.** Functionally independent columns of rat somatosensory barrel cortex revealed with voltage-sensitive dye imaging. *J Neurosci* 21: 8435–8446, 2001.
- Pouille F, Scanziani M.** Enforcement of temporal fidelity in pyramidal cells by somatic feed-forward inhibition. *Science* 293: 1159–1163, 2001.
- Prsa M, Dash S, Catz N, Dicke PW, Thier P.** Characteristics of responses of Golgi cells and mossy fibers to eye saccades and saccadic adaptation recorded from the posterior vermis of the cerebellum. *J Neurosci* 29: 250–262, 2009.
- Rancz EA, Ishikawa T, Duguid I, Chadderton P, Mahon S, Hausser M.** High-fidelity transmission of sensory information by single cerebellar mossy fibre boutons. *Nature* 450: 1245–1249, 2007.
- Rokni D, Llinás R, Yarom Y.** Stars and stripes in the cerebellar cortex: a voltage sensitive dye study. *Front Syst Neurosci* 1: Article 1, 2007.
- Shambes GM, Gibson JM, Welker W.** Fractured somatotopy in granule cell tactile areas of rat cerebellar hemispheres revealed by micromapping. *Brain Behav Evol* 15: 94–140, 1978.
- Sola E, Prestori F, Rossi P, Taglietti V, D'Angelo E.** Increased neurotransmitter release during long-term potentiation at mossy fibre–granule cell synapses in rat cerebellum. *J Physiol* 557: 843–861, 2004.
- Solinas S, Forti L, Cesana E, Mapelli J, De Schutter E, D'Angelo E.** Computational reconstruction of pacemaking and intrinsic electroresponsiveness in cerebellar Golgi cells. *Front Cell Neurosci* 1: Article 2, 2007a.
- Solinas S, Forti L, Cesana E, Mapelli J, De Schutter E, D'Angelo E.** Fast-reset of pacemaking and theta-frequency resonance patterns in cerebellar Golgi cells. *Front Cell Neurosci* 1: Article 4, 2007b.
- Staub C, De Schutter E, Knopfel T.** Voltage-imaging and simulation of effects of voltage- and agonist-activated conductances on soma-dendritic voltage coupling in cerebellar Purkinje cells. *J Comput Neurosci* 1: 301–311, 1994.
- Steuber V, Mittmann W, Hoebeek FE, Silver RA, DeZeeuw CI, Hausser M, De Schutter E.** Cerebellar LTD and pattern recognition by Purkinje cells. *Neuron* 54: 121–136, 2007.
- Sultan F.** Distribution of mossy fiber rosettes in the cerebellum of cat and mice: evidence for a parasagittal organization at the single fiber level. *Eur J Neurosci* 13: 2123–2130, 2001.
- Sultan F, Heck D.** Detection of sequences in the cerebellar cortex: numerical estimate of the possible number of tidal-wave inducing sequences represented. *J Physiol (Paris)* 97: 591–600, 2003.
- Tominaga T, Tominaga Y, Yamada H, Matsumoto G, Ichikawa M.** Quantification of optical signals with electrophysiological signals in neural activities of Di-4-ANEPPS stained rat hippocampal slices. *J Neurosci Methods* 102: 11–23, 2000.
- Torioka T.** Further consideration on pattern separability in a random neural net with inhibitory connections. *Biol Cybern* 36: 203–212, 1980.
- Tyrrell T, Willshaw D.** Cerebellar cortex. Its simulation and the relevance of Marr's theory. *Philos Trans R Soc Lond B Biol Sci* 336: 239–257, 1992.
- van Kan PL, Houk JC, Gibson AR.** Output organization of intermediate cerebellum of the monkey. *J Neurophysiol* 69: 57–73, 1993.
- Wu HS, Sugihara I, Shinoda Y.** Projection patterns of single mossy fibers originating from the lateral reticular nucleus in the rat cerebellar cortex and nuclei. *J Comp Neurol* 411: 97–118, 1999.
- Yae H, Elias SA, Ebner TJ.** Deblurring of 3-dimensional patterns of evoked rat cerebellar cortical activity: a study using voltage-sensitive dyes and optical sectioning. *J Neurosci Methods* 42: 195–209, 1992.
- Zhou WL, Ping Y, Wuskell JP, Loew LM, Antic SD.** Intracellular long wavelength voltage-sensitive dyes for studying the dynamics of action potentials in axons and thin dendrites. *J Neurosci Methods* 164: 225–239, 2007.